Interplay between the periodic potential modulation and random background scatterers in an antidot lattice

A. Dorn,[1] E. Bieri,[1] T. Ihn,[1] K. Ensslin,[1] D. D. Driscoll,[2] and A. C. Gossard[2]
[1]*Solid State Physics Laboratory, ETH Zürich, 8093 Zürich, Switzerland*
[2]*Materials Department, University of California Santa Barbara, Santa Barbara, California 93106, USA*
(Received 5 July 2004; published 28 January 2005)

Antidot lattices with top and back gate tunability allow the electronic transport properties of a sample to be studied at a constant electron density while the two-dimensional electron system is shifted in the *z* direction. The antidot potential is found to remain essentially unaltered in our sample during a constant density sweep, while other parameters such as the background mobility or wave function symmetry in the *z* direction vary. The impact of these changes on the classical commensurability peaks, the Aharonov-Bohm-type oscillations, and on a weak-localization-type feature around $B=0$ T are investigated. In addition, a peak splitting appears in oscillations superimposed on the main commensurability peak at high electron densities.

DOI: 10.1103/PhysRevB.71.035343 PACS number(s): 73.21.Cd, 73.23.Ad

I. INTRODUCTION

A two-dimensional electron system imprinted with a regular array of insulating islands is commonly called an antidot lattice.[1] These structures have attracted considerable experimental and theoretical interest over recent years.[2] In particular magnetoresistance peaks corresponding to commensurate cyclotron orbits enclosing 1,4,9, … , antidots have been observed in square antidot arrays[3] and explained in the context of classical billiard models.[4] At low temperatures, a fine oscillation with a periodicity of approximately one flux quantum through a cyclotron orbit is sometimes observed.[5,6] This feature has been explained by periodic orbit theory,[5,7,8] but interpretations in terms of a Hofstadter-type beating in the artificial band structure have also been proposed.[9] More recently, weak localization has also become an issue of interest in these systems.[11] The magnetoresistance effects mentioned above arise from the properties of the regular antidot potential modified by the presence of random background scatterers. However, in previous investigations the electron density and the overall mobility were not changed independently, so that contributions from the lattice and from the background scatterers were difficult to disentangle. In this paper we investigate this interplay by using antidot lattices with a top and back gate that allow us to tune the amount of background scatterers at constant electron sheet density.

II. SAMPLE

The sample discussed here (Fig. 1) was defined by local anodic oxidation of a GaAs heterostructure[12,13] with a two-dimensional electron system (2DES) 40 nm below the surface and a conducting back gate layer at a depth of 1.3 μm. The 2DES is insulated with respect to the back gate by layers of ErAs islands.[14] Patterning was performed with an atomic force microscope (AFM) operated in tapping mode in a controlled atmosphere with a humidity of 41% and at a temperature of 26.6 °C. Single antidots were oxidized by reducing the setpoint voltage and applying a 3 s/−24 V pulse to the conducting tip. The enclosing cavity was defined in a similar way with openings in the corners that serve as current and voltage leads (see Fig. 1). After patterning, the entire structure was covered with a TiAu layer that serves as a top gate. The high electronic quality of antidot lattices defined by this method has been demonstrated previously.[15]

First we consider theoretically how the amplitude of the antidot potential is expected to depend on the gate voltages. As can be seen by removing the oxide with an HCl dip etch, the oxide height closely resembles the corresponding etch depth.[13] This can be exploited to gain quantitative insight into the induced potential modulation. The inset in Fig. 2(b) shows the dependence of the electron sheet density, or equivalently Fermi energy, on the cap layer etch depth as calculated with a Poisson-Schrödinger solver[16] for a two-dimensional system. Using a fit function, this allows us to directly convert the oxide height profile of an antidot into the potential modulation of the underlying 2DES. This two-dimensional approach should be a good approximation since the lateral dimensions ($a=150$ nm) are considerably larger than the depth of the 2DES (~40 nm). If a voltage is applied to the top gate, there is an additional capacitive contribution arising from the modulated distance top gate-2DES [see Fig. 2(a)]. A plot of the resulting total potential modulation at a series of top gate voltages is presented in Fig. 2(b). As can be seen, the contribution from AFM lithography completely

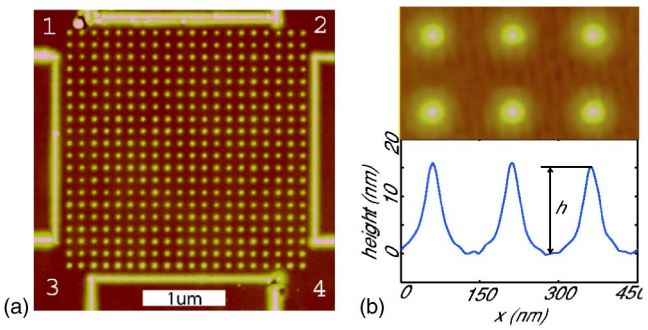

FIG. 1. (a) AFM scan of the structure under study. Bright areas are oxidized and correspond to depletion in the underlying 2DES. (b) Blowup illustrating the regularity and oxide height profile.

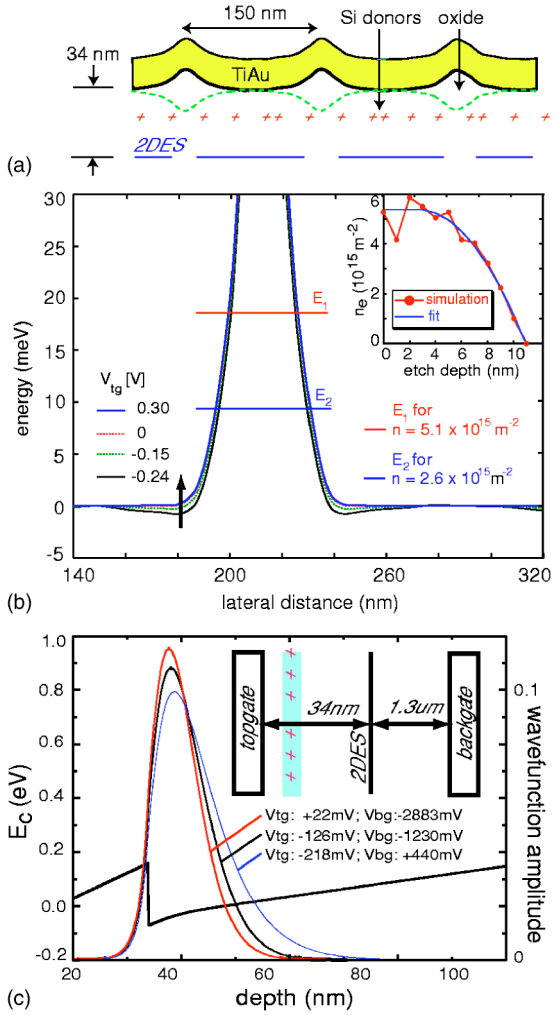

FIG. 2. (a) Schematic of a cross section through the sample. (b) Simulation of the induced potential profile taking capacitive contributions from the modulated top gate and the contribution from local anodic oxidation into account. Inset: Poisson-Schrödinger simulation of the electron sheet density as a function of cap-layer etch depth. (c) Poisson-Schrödinger simulation of the z component of the wave function for different top and back gate settings at a constant electron sheet density of 3.75×10^{15} m^{-2}. The Fermi energy is set to 0.

dominates, so that the overall potential profile remains essentially unaltered if the electron density is held constant. At a series of top gate voltages this can be achieved by applying suitable back gate voltages. The simulation does not take contributions from in-plane screening or from top gate metal induced strain or Fermi level pinning into account. Since these contributions should not be top or back gate voltage dependent, our assumption of a constant potential modulation should remain valid. However, as shown in Fig. 2(c), the position and symmetry of the z component of the 2DES wave function does change somewhat. As will be seen in the transport measurements discussed below, there is also a change in the strength of background scattering. This could be related to a depth-dependent defect density, or to different degrees of screening in the donor layer, as the top gate voltage is varied (see also Ref. 14).

III. COMMENSURABILITY PEAKS

The magnetoresistance is measured across diagonal 1 from corner 2 to 3, while the Hall voltage is measured across diagonal 2 between corners 1 and 4 [see Fig. 1(a)]. By applying voltages to the gates, the two-dimensional electron density can be tuned capacitively. The electron density in the lattice was determined from the position of a well-defined Shubnikov-de Haas minimum at a known filling factor. The availability of a top and a back gate in our samples enables us to sweep one gate and hold the electron density constant by applying suitable voltages to the second gate. This opens up a window on effects connected to changes in wave function symmetry and background mobility, as mentioned above, without having to take influences from a changing Fermi energy into account. Constant density sweeps were done by setting the top gate voltage to a fixed set of values and then adjusting the back gate voltage until the specified electron density was reached. The back gate voltage is not a well-defined parameter, because the ErAs islands between 2DES and back gate can become charged over time (see Ref. 14). This leads to an effective voltage offset to the back gate. However, if the back gate voltage is readjusted to give the same electron density at the same top gate voltage, the magnetoresistance was found to be virtually unchanged down to the smallest reproducible fluctuations. It is therefore sensible to define a state of the system in terms of a top gate voltage and electron density.

Figures 3(a) and 3(b) show magnetoresistance traces at a series of top and back gate settings for two different constant electron densities at 9 K. The overall resistance decreases and the commensurability features are better resolved at the higher electron density of 3.75×10^{15} m^{-2}. Within the constant density series at 3.75×10^{15} m^{-2} the electron mobility increases towards higher top gate voltages [Fig. 3(c)]. Only at the lower density of 2.62×10^{15} m^{-2} does the mobility increase again at the lowest top gate settings [Fig. 3(d)]. A possible explanation for the increase in mobility at high top gate voltages is a population of the donor layer (ionized Si atoms) with electrons, leading to improved screening. On the other hand, at very low top gate voltages, all the electrons have left the donor layer and the mobility increases again, because the 2DES is pushed away from the GaAs/GaAlAs interface. This reduces scattering off the ionized donor atoms and from defects close to the GaAs/AlGaAs interface.

The electron densities of $(3.75\pm0.05)\times10^{15}$ m^{-2} and $(2.62\pm0.05)\times10^{15}$ m^{-2} in the lattice correspond to values of $(4.25\pm0.05)\times10^{15}$ m^{-2} and $(3.25\pm0.05)\times10^{15}$ m^{-2}, respectively, in the unstructured leads. During a constant density series, the difference remains practically the same, but while going from the highest to the lowest density, the difference between lead and lattice increases from about 0.50×10^{15} m^{-2} to about 0.61×10^{15} m^{-2}. This is somewhat surprising, since the simulation in Fig. 2 predicts no saddle points between the antidots. A possible explanation is that we do not measure the maximum electron density between the antidots, but rather an averaged density over the entire cross-sectional area of the potential valley. This would also account for the larger difference at lower densities, where the potential slopes are less steep.

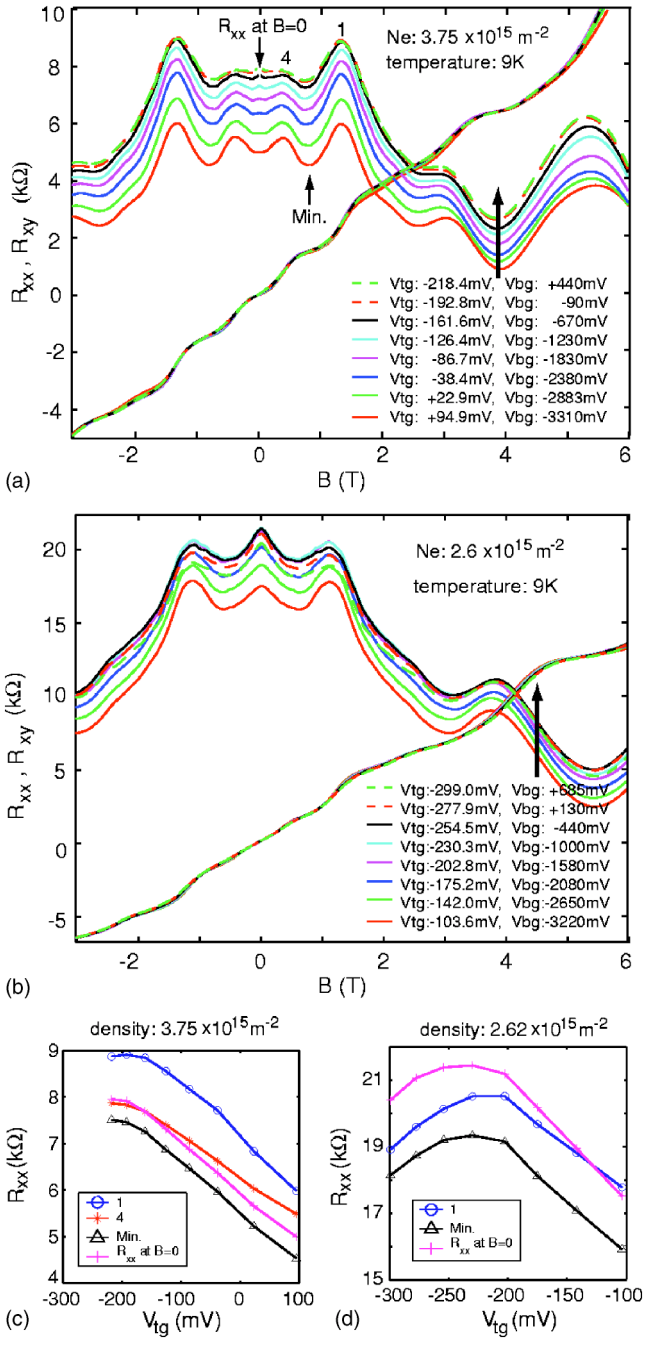

FIG. 3. Magnetoresistance between corners 2 and 3 at a series of top and back gate voltages at constant electron densities of (a) 3.75×10^{15} m^{-2} and (b) 2.6×10^{15} m^{-2}. (c) and (d) plot the top gate voltage dependence of the resistance at $B=0$ T, at the commensurability peaks around one and four antidots, and for the minimum between the two for both densities.

By comparing the settings for the top gate voltage and electron density in the lead with the same settings in an unstructured Hall bar with a known geometry, it is possible to extract the behavior of the background mobility in the wafer during a constant density series. The qualitative variation in background mobility in the wafer was found to be very similar to the longitudinal resistance changes at $B=0$ T in the lattice. This confirms our picture that, during a constant density sweep, the antidot potential remains essentially constant while the background mobility intrinsic to the wafer changes. As can be seen in Fig. 3(a), the commensurability peak around four antidots is more sensitive to changes in the mobility owing to its longer trajectory. In addition a pronounced resistance peak around $B=0$ T appears as the mobility decreases. The relatively high temperature of 9 K indicates that this effect is most likely caused by classical mechanisms. The observed peak shape is very similar to the negative magnetoresistance predicted for a classical Lorenz gas, where only hard scatterers are present,[17] possibly including a smooth random potential background as discussed by Mirlin *et al.*[18] As can be seen in Fig. 4(a), a temperature-dependent peak around $B=0$ T also arises with a height that is approximately proportional to the mobility at $B=0$ T [see Fig. 3(d)]. This feature can probably be attributed to a weak localization phenomena as discussed by Ihn *et al.*[10] or Yevtushenko *et al.*[11]

IV. AHARONOV-BOHM-TYPE OSCILLATIONS

We now turn to effects arising from phase coherence and interference of the conduction electrons. Aharonov-Bohm-type oscillations were detected at an electron density of 2.62×10^{15} m^{-2} at 1.7 K [Fig. 4(a)]. Measurements done with different lead configurations show the same features and exclude an irregularity in a single corner of the lattice as the sole source of the Aharonov-Bohm-type oscillations. This indicates that the effect is indeed a lattice property. The influence of changes in background mobility on the low temperature resistance fluctuations arising between 9 and 1.7 K can be seen in Fig. 4(a). Surprisingly the Aharonov-Bohm-type oscillations are most pronounced at the lowest mobility [see highlighted trace in Fig. 4(b) and resistance dependence Fig. 3(d)]. This observation is put on a more quantitative basis in Fig. 4(d), where the fast Fourier transforms (FFT's) of the traces plotted in Fig. 4(a), are shown. The FFT of the trace at the lowest mobility has the highest and sharpest peak at a frequency corresponding to a flux quantum through a circle with a diameter of $a=150$ nm. This behavior has been predicted by Ando *et al.*[8] as a consequence of the suppression of contributions from larger periodic orbits and more complex band-structure effects by background scatterers. An analysis of the minima in the trace at the lowest mobility is presented in Figs. 4(b) and 4(c). A period of 0.23 T is extracted, that matches the value of 0.235 T for a flux quantum through a circular orbit with a diameter of $a=150$ nm. From this we can identify the periodic orbit around 1 antidot as the origin of the oscillations in accordance with numerical simulations.[5,7,19] In contrast, a beating corresponding to a flux quantum through the square unit cell would have a periodicity of 0.183 T.

There is no smooth transition from the Aharonov-Bohm to the Shubnikov-de Haas effect in the 150 nm sample, as has been observed in arrays with larger lattice constants.[5,15] Instead, the Aharonov-Bohm-type oscillations extend up to 4 T with high periodicity and coexist with the Shubnikov-de Haas effect. This is remarkable since, in contrast to earlier reports, the commensurability peak around one antidot and

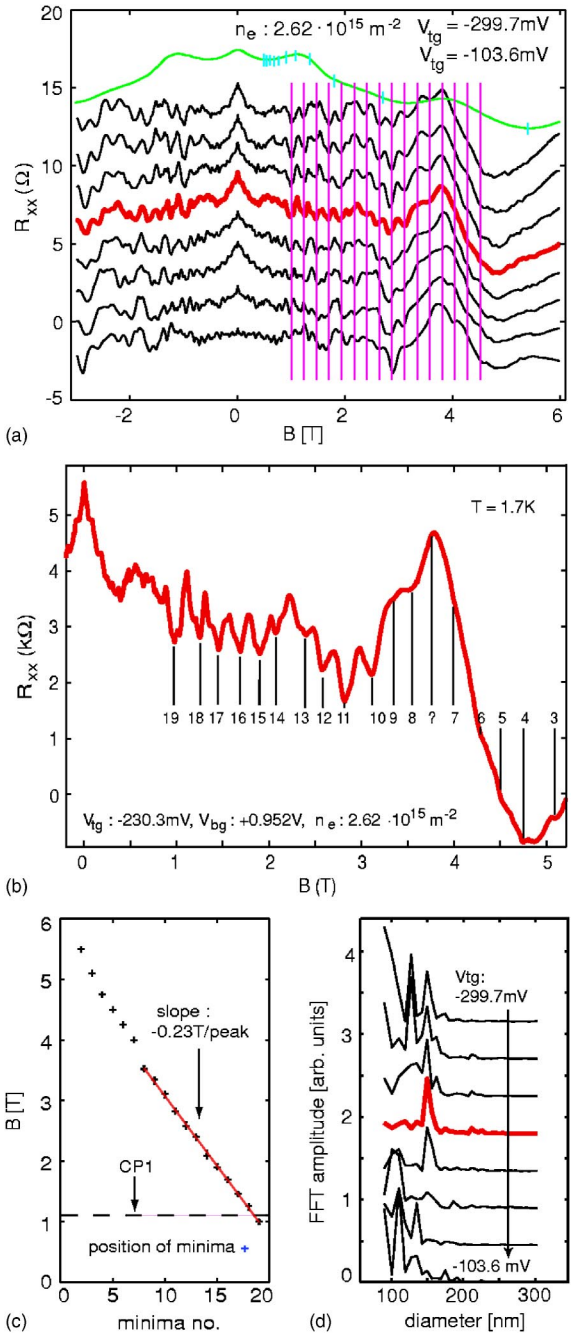

FIG. 4. (a) Difference in the magnetoresistance between a series of constant density sweeps (2.62×10^{15} m^{-2}, see Fig. 3) taken at 9 and at 1.7 K. The resistance was measured from corner 2 to 3. The vertical lines have a spacing of 0.235 T corresponding to a flux quantum through a circular orbit with a diameter of $a=150$ nm. The uppermost trace (resistance not to scale) is a 9 K sweep with a clear commensurability peak around one antidot, the short vertical lines indicating the positions of Shubnikov-de Haas minima. (b) Numbered Aharonov-Bohm minima of the trace highlighted in (a). (c) Magnetic field values at the numbered minima shown in (b). From the slope an average spacing of 0.23 T is extracted. (d) Fourier transform of the traces in (a). The highlighted trace with the sharpest peak corresponds to the trace with the lowest mobility highlighted in (a) and (b).

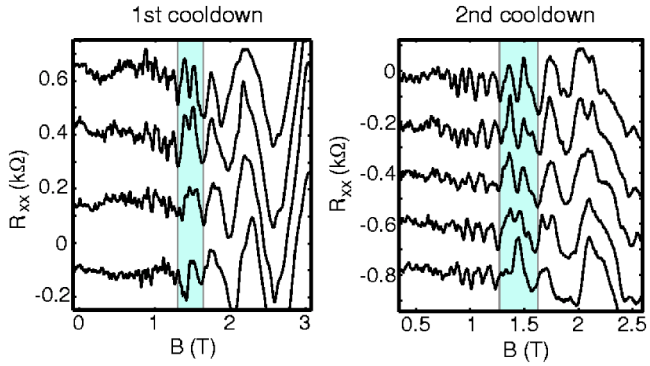

FIG. 5. Difference between traces at 1.7 and 9 K for a constant density series at 5.1×10^{15} m^{-2} for two different cooldowns. The shaded region highlights a peak superimposed on the main commensurability peak that splits while the gates are tuned.

hence the corresponding classical cyclotron orbit is located at a much smaller magnetic field below 1.5 T [see Fig. 4(a)]. In an intuitive picture this might be attributed to a more rigid electronic band structure originating from the lower number of modes between two antidots at smaller lattice constants.

V. PEAK SPLITTING

An unexpected feature was found in the low temperature magnetoresistance traces taken at high electron densities. The difference between a 9 and a 1.7 K series taken with the same gate settings at an electron density of 5.1×10^{15} m^{-2} is plotted in Fig. 5. A peak arising towards lower temperatures superimposed on the main commensurability maximum at about 1.5 T splits as the 2DES is shifted. This effect has not been reported previously and could have several possible interpretations: (a) Universal conductance fluctuations are known to change when the disorder configuration is altered. This could be the case when the 2DES is shifted in the z direction at different top and back gate settings, but two points make this interpretation seem unlikely. The peak splitting feature is about a factor of 5 larger in amplitude than the magnetic-field-dependent fluctuations around $B=0$ T and does not appear to be random in nature. Secondly the feature is present in two different cooldowns. (b) Differences in the periodicity of the Shubnikov-de Haas oscillations in the lattice and in the leads resulting from small variations in the electron sheet density could be a cause. However, the exact matching of the Shubnikov-de Haas maxima and minima at higher magnetic fields practically excludes this possibility. (c) The splitting could be related to the Aharonov-Bohm-type oscillations or the $h/2e$ oscillations appearing at lower densities, however, no real B periodicity over several peaks is observed. In a band structure picture the peak splitting could also be attributed to a disorder induced opening or closing of a band gap. (d) Spin orbit coupling increases towards higher electron densities. Since not only the electron mobility but also the wave function symmetry in the z direction changes while the 2DES is shifted, this could be a factor. However spin-orbit interactions are known to be weak in n-type GaAs.

Measurements focusing on weak anti-localization below 1 K could yield insight into this interesting possibility.

VI. CONCLUSIONS

Antidot arrays defined by AFM lithography have an electronic quality comparable to the best lattices fabricated by other techniques. The finite size of the arrays seems to have no significant influence on the magnetotransport properties. As in earlier reports, the classical commensurability peaks are well described by theory.[4]

Aharonov-Bohm-type oscillations were detected at low electron densities. The periodicity of 0.23 T precisely matches a flux quantum through a circular orbit with a diameter of $a=150$ nm (0.235 T), which can clearly be distinguished from a flux quantum through the square unit cell (0.183 T). It is surprising that the oscillations persist up to 4 T, more than *twice* the magnetic field of the main commensurability peak, without changing frequency. Instead of a smooth transition to the Shubnikov-de Haas effect, the two oscillations coexist, which is in marked contrast to earlier reports.[5,15] In periodic orbit theory, classical orbits would strongly contract with increasing magnetic field, especially if the small antidot diameter of only about 35 nm (from simulation) is compared to the lattice constant of $a=150$ nm. Under these conditions it is possibly more adequate to think of the electron wave functions as being bound to the antidots with concentric states similar to edge states in the quantum Hall regime. The conductance is then modulated by the overlapping states in the valleys that form an extended network. This would also explain the observed constant period of 0.23 T up to very high magnetic fields.

In mobility dependent sweeps we found the most pronounced Aharonov-Bohm-type oscillations at the lowest electron mobilities. According to Uryu and Ando[19] this can be interpreted as a washing out of more complex band structure effects in the presence of an increased amount of random background scatterers. Aharonov-Altschuler-Spivak oscillations around $B=0$ T were also present in some traces, but were more sensitive to changes in parameters than the Aharonov-Bohm-type oscillations.

An unexpected peak splitting effect superimposed on the main commensurability peak was observed as the 2DES was shifted at high constant electron densities.

ACKNOWLEDGMENT

This work was supported by the Schweizerischer Nationalfonds.

[1] K. Ensslin and P. M. Petroff, Phys. Rev. B **41**, 12 307 (1990).
[2] For a review see, e.g., R. Schuster and K. Ensslin, Festkoerperprobleme **34**, 195 (1994).
[3] D. Weiss, M. L. Roukes, A. Menschig, P. Grambow, K. v. Klitzing, and G. Weimann, Phys. Rev. Lett. **66**, 2790 (1991).
[4] R. Fleischmann, T. Geisel, and R. Ketzmerick, Phys. Rev. Lett. **68**, 1367 (1992).
[5] D. Weiss, K. Richter, A. Menschig, R. Bergmann, H. Schweizer, K. v. Klitzing, and G. Weimann, Phys. Rev. Lett. **70**, 4118 (1993).
[6] R. Schuster, K. Ensslin, D. Wharam, S. Kühn, J. P. Kotthaus, G. Böhm, W. Klein, G. Tränkle, and G. Weimann, Phys. Rev. B **49**, 8510 (1994).
[7] G. Hackenbroich and F. Von Oppen, Europhys. Lett. **29**, 151 (1995).
[8] T. Ando, S. Uryu, and S. Ishizaka, Jpn. J. Appl. Phys., Part 1 **38**, 308 (1999).
[9] R. B. S. Oakshott and A. MacKinnon, J. Phys.: Condens. Matter **6**, 1519 (1994).
[10] T. Ihn, M. Mosberger, R. Schuster, and K. Ensslin, in Proceedings of the 24th ICPS, Jerusalem, Israel, 1998 ♯ VA.31 on CD-ROM (ISBN 981-02-40309) (1999).
[11] O. Yevtushenko, G. Lütjering, D. Weiss, and K. Richter, Phys. Rev. Lett. **84**, 542 (2000),
[12] T. Heinzel, R. Held, S. Lüscher, K. Ensslin, W. Wegscheider, and M. Bichler, Physica E (Amsterdam) **9**, 84 (2001).
[13] A. Fuhrer, A. Dorn, S. Lüscher, T. Heinzel, K. Ensslin, W. Wegscheider, and M. Bichler, Superlattices Microstruct. **31**, 19, (2002).
[14] A. Dorn, M. Peter, S. Kicin, T. Ihn, K. Ensslin, D. Driscoll, and A. C. Gossard, Appl. Phys. Lett. **82**, 2631 (2003).
[15] A. Dorn, M. Sigrist, A. Fuhrer, T. Ihn, T. Heinzel, K. Ensslin, W. Wegscheider, and M. Bichler, Appl. Phys. Lett. **80**, 252 (2002).
[16] The complete structure was calculated self-consistently with a one-dimensional Poisson-Schrödinger solver, copyright 1995 by G. Snider, Department of Electrical Engineering, University of Notre Dame, Notre Dame, IN 46556, http://www.nd.edu/~gsnider/
[17] A. V. Bobylev, Frank A. Maaø, Alex Hansen, and E. H. Hauge, Phys. Rev. Lett. **75**, 197 (1995).
[18] A. D. Mirlin, D. G. Polyakov, F. Evers, and P. Wölfle, Phys. Rev. Lett. **87**, 126805 (2001).
[19] S. Uryu, T. Ando, Physica B **256–258**, 388 (1998).